# A NON-CONTACT ELECTRODE FOR MEASUREMENT OF ELECTROCARDIOGRAPHY

by

**Quan Tao**

Bachelor of Science, Nanjing University of Aeronautics and Astronautics, China, 2009

Submitted to the Graduate Faculty of

Swanson School of Engineering in partial fulfillment

of the requirements for the degree of

Master of Science in Electrical Engineering

University of Pittsburgh

2011

UNIVERSITY OF PITTSBURGH

SWANSON SCHOOL OF ENGINEERING

This thesis was presented

by

Quan Tao

It was defended on

November 18th, 2011

and approved by

Guangyong Li, Ph. D., Assistant Professor, Departmental of Electrical and Computer Engineering

Zhi-Hong Mao, Ph. D., Associate Professor, Departmental of Electrical and Computer Engineering

Robert J. Sclabassi, Ph. D., Professor Emeritus, Department of Neurological Surgery, Department of Electrical and Computer Engineering

Thesis Advisor: Mingui Sun, Ph. D., Professor, Department of Neurological Surgery, Department of Electrical and Computer Engineering

**A NON-CONTACT ELECTRODE FOR MEASUREMENT OF ELECTROCARDIOGRAPHY**

Quan Tao, M.S.

University of Pittsburgh, 2011

Heart disease has become a widespread epidemic threatening the health of millions of Americans and costing billions of dollars in therapy. In heart disease treatment, an effective heart monitoring technique is desired. In this thesis, a novel non-contact electrode was designed and fabricated to measure electrocardiography (ECG) based on widely used spherical volume conductor model. This model has been demonstrated to have a closed-form solution, which enables measurement of electric potential with capacitive electrode. Finite element analysis performed in Ansoft Maxwell software showed the feasibility of using an X-antenna to represent the ideal current dipole. The capacitive electrode we designed consists of two small sensing electrodes and a large reference electrode. This electrode measured promising signals for both direct and non-contact tests on spherical volume conductor model. Experiments were performed to find the best orientation and location for the electrode to measure the most significant signals on the surface of the sphere. Our electrode can also showed positive results in realizing both direct and non-contact measurement of the real ECG signals.

## TABLE OF CONTENTS

## LIST OF TABLES

## LIST OF FIGURES

## PREFACE

An effective technique of heart monitoring is critical in heart disease treatment. Although conventional 12-lead ECG is able to provide qualified ECG signals, the uncomfortable skin-contact and complicated measurement process limit its application for in-home use. Capacitive electrode has shown the ability to measure ECG signals through cloth. However, the theoretical analysis of this contactless measurement and the electric potential produced by heart activities are seldom investigated. It was my advisor, Professor Mingui Sun, who suggested a combination of the widely used spherical volume conductor model and the capacitive measurement theory. This suggestion stimulated my further work on finding out the theoretical solution of spherical volume conductor model, simulating the model, and designing a novel non-contact electrode to measure ECG signals. Specially, this thesis will support the usefulness of the suggestion.

More importantly, I would like to take this opportunity to direct my sincere thanks to Professor Mingui Sun, Professor Zhi-Hong Mao, Professor Robert J. Sclabassi, Professor Wenyan Jia, and all my labmates for their valuable guidance and suggestions. My thanks also go to my parents, Mr. Guangzhong Tao and Ms. Fengzhen Chen, for their constant understanding and encouraging support during the course of this research.

# 1.0 INTRODUCTION

The heart, a 4-chamber organ, plays a critical role in supplying blood throughout the body. However, congenial reasons as well as inappropriate lifestyles like unhealthy diet and being physically inactivate increase the risk of a series of heart disease including coronary heart disease, cardiomyopathy, cardiovascular disease, arrhythmia, and heart failure. Heart disease is a major threat to the health of millions of Americans and costs billions of dollars in therapy. Since 2007, it has become the leading cause of death in the United States, accounting 25.4% of total deaths each year [1].

In studies of heart disease and potential treatment, accurate display and understanding of heart activity are essential. Located in the right atrium, a small collection of specific heart cells called sinus node serves as the heart's "natural pacemaker". When the sinus node discharges, the two atria contract and an electrical pulse travels through the atria to reach the atrioventricular (AV) node. The AV node works as a relay point to further propagate the electrical pulse to the ventricles, causing them to contract and pump blood. The electrical system of the heart enables the physicians to record the heart activity using the electrocardiography (ECG) technique. A typical ECG signal is shown in Figure 1 [2]. Atrial contractions show up as the P wave, while ventricular contractions are illustrated by a series of three waves, known as the QRS complex. The last T wave reflects the electrical activity produced when the ventricles are recharging for

the next contraction (repolarization). The recorded ECG signals help doctors to recognize the abnormality of the heart and to determine treatment options for the patients.

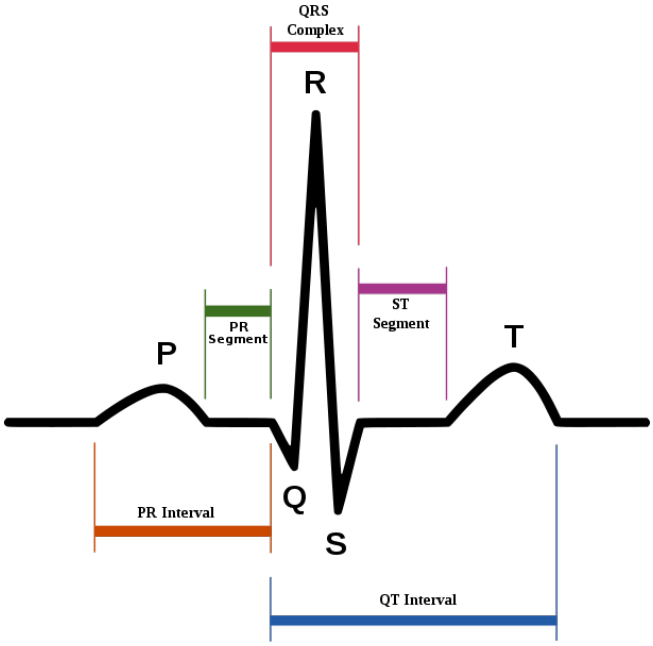


**Figure 1.** A typical ECG signal

The most common method of acquiring the ECG signal is the standard 12-lead ECG. Ten Ag/AgCl electrodes are fixed on the well-defined locations on the limbs and the torso through galvanic contact with the skin. A combination of an electrolyte with the electrode is able to optimize the impedance between the electrode and the skin, providing the voltage differences between these electrodes, namely, the standard leads. However, because of the complicate process, the conventional 12-lead ECG can only be performed in hospitals or clinics by professional physicians. For those patients with chronic heart diseases, an easy-handling mobile device to measure the ECG signals is highly needed for long-time examination and treatment. Moreover, the inconvenience and discomfort of the skin-contact electrodes also limit the usage of the conventional ECG technique.

Compared to the conventional galvanic electrode, a capacitive electrode can measure the surface potential without galvanic contact with the skin. For wearable monitoring devices, this

provides numerous advantages since capacitive electrodes simplify the measurement process, are insensitive to the variation of the skin conditions, and can be embedded comfortably within cloths. With recent rapid advances in electrical engineering, some researchers have incorporated capacitive electrodes in their mobile devices to monitor the heart activity [3-5]. Oehler et al. fabricated a mobile device containing a 15-electrode array to measure ECG signals [3, 4]. Chi et al.'s device consists of two connecting PCB board, one of which contains a solid insulated copper fill and behaves like normal capacitive electrode [5]. In all these approaches, the measuring devices include high-cost, complicate circuits which are not easy to fabricate. Moreover, when designing capacitive electrodes, people seldom consider the theoretical study of the electric potential produced by the heart activities. However, fundamental understanding of the theoretical basis of electrical current and potential within both the heart and the surrounding tissue is extremely important to optimize ECG measurement systems.

This thesis aims to propose a novel capacitive electrode to measure ECG signals. The electric potential generated by the heart was theoretically investigated based on spherical volume conductor model. A dipole antenna was designed to represent the ideal current dipole. Finite element simulation was implemented to demonstrate the feasibility of this antenna design. Capacitive electrodes consisting of two small sensing electrodes and one large reference electrode were constructed. Besides the direct measurement, our capacitive electrodes showed promising results when measuring electric potential on the surface of a conductive spherical torso model through several layers of cloths. We performed several experiments and found the best location and orientation for the electrodes to measure the most significant signals, which matches our theoretical results. Moreover, our capacitive electrodes showed positive

performance in both direct and non-contact measurement of the real ECG signals from the human heart.

Our design was motivated by the theoretical spherical volume conductor model and was supported by finite element simulation. The experiments have shown promising results in direct and non-contact measurements of electric potentials generated either from the spherical volume conductor model or the real heart. Moreover, because of the simple structure as well as inexpensive fabrication cost, our capacitive electrodes have great potential in the application to handheld devices for real-time cardiac monitoring.

# 2.0 BACKGROUND

## 2.1 SPHERICAL VOLUME CONDUCTOR MODEL

Spherical volume conductor model, proposed by Helmholtz, is widely used in the analysis of ECG problems to explain the electric activities of the heart. Although a conducting sphere is a rough approximation of the torso, the electric field produced by the heart in local region can be modeled as being generated by a current dipole source inside a homogeneous conducting sphere [6]. In ECG study, interior potential tells the information of the electric source inside the heart, while the potential on the surface of the sphere and the exterior potential enable the direct and non-contact measurement of ECG. Therefore, we are interested in the electric potential produced by the current dipole in space. However, the distribution of the electric field produced by a given spherical volume conductor, also known as the forward problem in ECG, remained to be a challenging task. Guided by Wilson and Bayley's pioneering contribution, many researchers have performed extensive investigations on solving the forward problem [6]. For example, the Legendre series solutions were derived for multi-shell spherical volume conductor model [7, 8]. However, expressed as the sum of infinite polynomials, these series solutions are sophisticated and computationally expensive in the simulation study [9]. Fortunately, some researchers have made extraordinary contributions to the derivation of an analytical solution for the spherical

volume conductor model, which brings significant benefits to both simulation and experimental studies on ECG applications [10-12].

### 2.1.1 Mathematical Description of Electric Potential

Quasi-static theory of electromagnetism assumes the electric and the magnetic fields are time-invariant. Then Faraday's law of induction reduces to

$$\nabla \times \boldsymbol{E}(\boldsymbol{r}) = \boldsymbol{0} \tag{2.1}$$

and Maxwell-Ampere equation becomes

$$\nabla \times \boldsymbol{B}(\boldsymbol{r}) = \mu_0 \boldsymbol{J}(\boldsymbol{r}) \tag{2.2}$$

and Gauss's law for magnetism is written as

$$\nabla \cdot \boldsymbol{B}(\boldsymbol{r}) = 0 \tag{2.3}$$

where $\boldsymbol{E}(\boldsymbol{r})$ is the electric field, $\boldsymbol{B}(\boldsymbol{r})$ is the magnetic induction field, $\boldsymbol{J}(\boldsymbol{r})$ is the total current density, and constant $\mu_0$ is the magnetic permeability of the medium [13].

For a conductive medium with conductivity $\sigma$, the total current density $\boldsymbol{J}(\boldsymbol{r})$ consists of the induction current $\boldsymbol{J}^i(\boldsymbol{r})$ and the primary current $\boldsymbol{J}^p(\boldsymbol{r})$

$$\boldsymbol{J}(\boldsymbol{r}) = \boldsymbol{J}^i(\boldsymbol{r}) + \boldsymbol{J}^p(\boldsymbol{r}). \tag{2.4}$$

The induction current $\boldsymbol{J}^i(\boldsymbol{r})$ is correlated with the electric field $\boldsymbol{E}(\boldsymbol{r})$

$$\boldsymbol{J}^i(\boldsymbol{r}) = \sigma \boldsymbol{E}(\boldsymbol{r}). \tag{2.5}$$

In ECG study, a current dipole is a widely used concept to approximate a localized primary current. The current dipole with moment $\boldsymbol{Q}$ can be treated as a concentration of $\boldsymbol{J}^p(\boldsymbol{r})$ to a single point $\boldsymbol{r}_0$. Mathematically, we have

$$\boldsymbol{J}^p(\boldsymbol{r}) = \boldsymbol{Q}\delta(\boldsymbol{r} - \boldsymbol{r}_0) \tag{2.6}$$

where $\delta$ is the Dirac measure.

Since the electric field is irrotational, it is convenient to introduce the concept of electric potential $u(\boldsymbol{r})$, such that

$$\boldsymbol{E}(\boldsymbol{r}) = -\nabla u(\boldsymbol{r}). \tag{2.7}$$

Taking the divergence on both sides on Equation (2.2) produces the conservation law

$$\nabla \cdot \boldsymbol{J}(\boldsymbol{r}) = 0 \tag{2.8}$$

which turns to a partial differential equation in the view of Equations (2.4), (2.5), and (2.7)

$$\nabla \cdot [\sigma \nabla u(\boldsymbol{r})] = \nabla \cdot \boldsymbol{J}^p(\boldsymbol{r}). \tag{2.9}$$

Particularly, for homogeneous conductors the electric potential $u(\boldsymbol{r})$ needs to satisfy

$$\sigma \Delta u(\boldsymbol{r}) = \begin{cases} \nabla \cdot \boldsymbol{J}^p(\boldsymbol{r}), & r \in supp\, \boldsymbol{J}^p(\boldsymbol{r}) \\ 0, & r \notin supp\, \boldsymbol{J}^p(\boldsymbol{r}) \end{cases} \tag{2.10}$$

where $\Delta$ is the Laplace operator.

For the typical spherical volume conductor model, there is an interface $S$ separating the interior conductive region $V_1$ and the exterior nonconductive region $V_2$, depicted in Figure 2. The interior electric potential $u_1(\boldsymbol{r})$ and the exterior electric potential $u_2(\boldsymbol{r})$ obey the boundary conditions

$$u_1(\boldsymbol{r}) = u_2(\boldsymbol{r}), \qquad \text{on } S \tag{2.11}$$

$$\sigma_1 \partial_n u_1(\boldsymbol{r}) = \sigma_2 \partial_n u_2(\boldsymbol{r}), \qquad \text{on } S \tag{2.12}$$

where $\partial_n$ denotes the normal derivative. Hence the electric potential remains continuous on the boundaries while its normal derivative follows Equation (2.12) in order to preserve the continuity of the normal components of the induction current. Moreover, since there is no induction current in the nonconductive region, Equation (2.12) reduces to

$$\partial_n u_1(\boldsymbol{r}) = 0, \qquad \text{on } S. \tag{2.13}$$

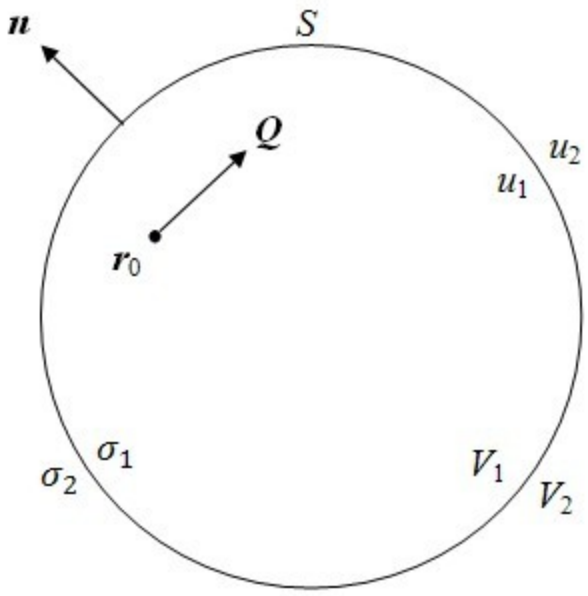


**Figure 2.** 2D geometry of spherical volume conductor model

### 2.1.2 Electric Potential of Spherical Volume Conductor

For a spherical homogeneous conductor with radius $a$ and conductivity $\sigma$, there is a current dipole with moment $\boldsymbol{Q}$ at an arbitrary location $\boldsymbol{r}_0$ inside the sphere, shown in Figure 3. The electric potential at any point $P$ needs to be determined. According to the pre-knowledge in Section **2.1.1**, the interior electric potential $u^-(\boldsymbol{r})$ is governed by a Neumann problem

$$\sigma \Delta u^-(\boldsymbol{r}) = \boldsymbol{Q} \cdot \nabla \delta(\boldsymbol{r} - \boldsymbol{r}_0), \qquad |\boldsymbol{r}| < a \tag{2.14}$$

$$\partial_n u^-(\boldsymbol{r}) = 0, \qquad |\boldsymbol{r}| = a. \tag{2.15}$$

Once this problem is solved, the value of $u^-(\boldsymbol{r})$ on $|\boldsymbol{r}| = a$ is used to solve the exterior Dirichlet problem

$$\Delta u^+(\boldsymbol{r}) = 0, \qquad |\boldsymbol{r}| > a \tag{2.16}$$

$$u^+(\boldsymbol{r}) = u^-(\boldsymbol{r}), \qquad |\boldsymbol{r}| = a \tag{2.17}$$

$$u^+(\boldsymbol{r}) = O\left(\frac{1}{r^2}\right), \qquad \boldsymbol{r} \to +\infty. \tag{2.18}$$

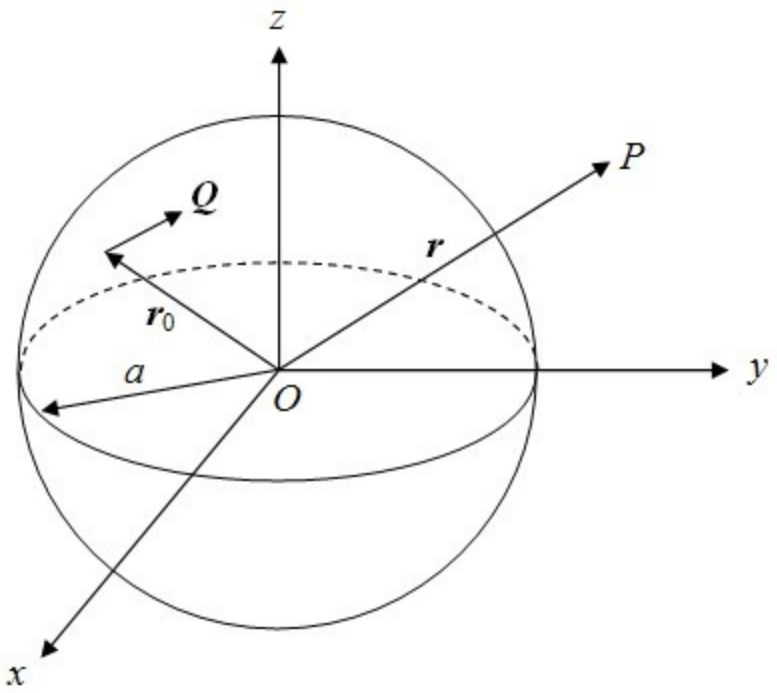


**Figure 3.** 3D description of spherical volume conductor model

Since the potential is generated by the current dipole source, the interior Neumann problem assumes $u^-(\boldsymbol{r})$ has the form

$$u^-(\boldsymbol{r}) = \frac{1}{4\pi\sigma}\boldsymbol{Q}\cdot\frac{\boldsymbol{r}-\boldsymbol{r}_0}{|\boldsymbol{r}-\boldsymbol{r}_0|^3} + w(\boldsymbol{r}) \tag{2.19}$$

where $w(\boldsymbol{r})$ can be expanded in spherical harmonic form. Consider the relation

$$\frac{\boldsymbol{r}-\boldsymbol{r}_0}{|\boldsymbol{r}-\boldsymbol{r}_0|^3} = \boldsymbol{\nabla}_{\boldsymbol{r}_0}\frac{1}{|\boldsymbol{r}-\boldsymbol{r}_0|} \tag{2.20}$$

Equation (2.19) can be rewritten as

$$u^-(\boldsymbol{r}) = \frac{1}{4\pi\sigma}\boldsymbol{Q}\cdot\boldsymbol{\nabla}_{\boldsymbol{r}_0}\left[\frac{1}{|\boldsymbol{r}-\boldsymbol{r}_0|} + \sum_{n=0}^{\infty}\sum_{m=-n}^{n}A_n^m r^n Y_n^m(\hat{\boldsymbol{r}})\right]. \tag{2.21}$$

where $Y_n^m(\hat{\boldsymbol{r}})$ denote the complex spherical harmonics, $A_n^m$ are the coefficients which can be calculated by the boundary condition in Equation (2.15). The introduction of Laplace expansion

$$\frac{1}{|\boldsymbol{r}-\boldsymbol{r}_0|} = \sum_{n=0}^{\infty}\frac{{r_0}^n}{r^{n+1}}P_n(\hat{\boldsymbol{r}}\cdot\hat{\boldsymbol{r}}_0) \tag{2.23}$$

and addition theorem

$$P_n(\hat{\boldsymbol{r}}\cdot\hat{\boldsymbol{r}}_0)=\frac{4\pi}{2n+1}\sum_{m=-n}^{n}Y_n^m(\hat{\boldsymbol{r}}_0)^*Y_n^m(\hat{\boldsymbol{r}}) \tag{2.24}$$

gives

$$\frac{1}{|\boldsymbol{r}-\boldsymbol{r}_0|}=\sum_{n=0}^{\infty}\sum_{m=-n}^{n}\frac{4\pi}{2n+1}\frac{{r_0}^n}{r^{n+1}}Y_n^m(\hat{\boldsymbol{r}}_0)^*Y_n^m(\hat{\boldsymbol{r}}) \tag{2.25}$$

where $r$ and $r_0$ are the magnitude of $\boldsymbol{r}$ and $\boldsymbol{r}_0$, respectively, $P_n(\hat{\boldsymbol{r}}\cdot\hat{\boldsymbol{r}}_0)$ is the Legendre polynomial of degree $n$, $Y_n^m(\hat{\boldsymbol{r}}_0)^*$ denotes the conjugate of $Y_n^m(\hat{\boldsymbol{r}}_0)$. We plug in Equation (2.25) to Equation (2.21) and consider the boundary condition in Equation (2.15), the coefficient $A_n^m$ is able to be determined, which leads to the solution

$$u^-(\boldsymbol{r})=\frac{1}{\sigma}\boldsymbol{Q}\cdot\boldsymbol{\nabla}_{\boldsymbol{r}_0}\left[\sum_{n=1}^{\infty}\sum_{m=-n}^{n}\frac{1}{2n+1}\left(\frac{{r_0}^n}{r^{n+1}}+\frac{n+1}{n}\frac{{r_0}^n r^n}{a^{2n+1}}\right)Y_n^m(\hat{\boldsymbol{r}}_0)^*Y_n^m(\hat{\boldsymbol{r}})\right] \tag{2.26}$$

Using Equations (2.23) and (2.24), we obtain

$$u^-(\boldsymbol{r})=\frac{1}{4\pi\sigma}\boldsymbol{Q}\cdot\boldsymbol{\nabla}_{\boldsymbol{r}_0}\left[\frac{1}{|\boldsymbol{r}-\boldsymbol{r}_0|}+\sum_{n=1}^{\infty}\frac{n+1}{n}\frac{{r_0}^n r^n}{a^{2n+1}}P_n(\hat{\boldsymbol{r}}\cdot\hat{\boldsymbol{r}}_0)\right] \tag{2.27}$$

Since any function *f(ρ)* on the interval -1 ≤ $\rho$ ≤ 1 can be expanded in terms of Legendre polynomials, it is possible to find a unique *f(ρ)* to simplify the series part in Equation (2.27). Define the function

$$f(\rho)=\sum_{n=1}^{\infty}\frac{\rho^n}{n}P_n(x) \tag{2.28}$$

where $x=\hat{\boldsymbol{r}}\cdot\hat{\boldsymbol{r}}_0$ and $\rho=r_0/a<1$, which satisfies the initial conditions

$$\rho f'(\rho)=\frac{1}{\sqrt{1-2x\rho+\rho^2}}-1, \qquad f(0)=0. \tag{2.29}$$

*f(ρ)* has the solution

$$f(\rho)=-ln\left[\frac{1-x\rho+\sqrt{1-2x\rho+\rho^2}}{2}\right]. \tag{2.30}$$

Equation (2.27) is rewritten as

$$u^-(\boldsymbol{r})=\frac{1}{4\pi\sigma}\boldsymbol{Q}\cdot\boldsymbol{\nabla}_{\boldsymbol{r}_0}\left[\frac{1}{|\boldsymbol{r}-\boldsymbol{r}_0|}+\sum_{n=1}^{\infty}\frac{{r_0}^n r^n}{a^{2n+1}}P_n(\hat{\boldsymbol{r}}\cdot\hat{\boldsymbol{r}}_0)+\sum_{n=1}^{\infty}\frac{1}{n}\frac{{r_0}^n r^n}{a^{2n+1}}P_n(\hat{\boldsymbol{r}}\cdot\hat{\boldsymbol{r}}_0)\right]$$

$$= \frac{1}{4\pi\sigma}\boldsymbol{Q}\cdot\boldsymbol{\nabla}_{\boldsymbol{r}_0}\left[\frac{1}{|\boldsymbol{r}-\boldsymbol{r}_0|}+a\sum_{n=1}^{\infty}\frac{{r_0}^n r^n}{(a^2)^{n+1}}P_n(\hat{\boldsymbol{r}}\cdot\hat{\boldsymbol{r}}_0)+\frac{1}{a}\sum_{n=1}^{\infty}\frac{(\frac{rr_0}{a^2})^n}{n}P_n(\hat{\boldsymbol{r}}\cdot\hat{\boldsymbol{r}}_0)\right] \quad (2.31)$$

The first series part can be simplified by Laplace expansion in Equation (2.23), while the second series part is able to be converted to the analytic expression in view of Equation (2.30). Finally, the interior electric potential is written in the following closed form:

$$u^{-}(\boldsymbol{r}) = \frac{1}{4\pi\sigma}\boldsymbol{Q}\cdot\boldsymbol{\nabla}_{\boldsymbol{r}_0}\left[\frac{1}{|\boldsymbol{r}-\boldsymbol{r}_0|}+\frac{a}{|a^2\hat{\boldsymbol{r}}-r\boldsymbol{r}_0|}\right.$$

$$\left.-\frac{1}{a}ln\frac{1}{2}\left(1-\frac{rr_0}{a^2}\hat{\boldsymbol{r}}\cdot\hat{\boldsymbol{r}}_0+\sqrt{1-2\frac{rr_0}{a^2}\hat{\boldsymbol{r}}\cdot\hat{\boldsymbol{r}}_0+\frac{r^2{r_0}^2}{a^4}}\right)\right]$$

$$= \frac{1}{4\pi\sigma}\boldsymbol{Q}\cdot\boldsymbol{\nabla}_{\boldsymbol{r}_0}\left[\frac{1}{|\boldsymbol{r}-\boldsymbol{r}_0|}+\frac{1}{|t^2\boldsymbol{r}-\boldsymbol{r}_0|}-\frac{1}{a}ln\frac{1}{2at}(\hat{\boldsymbol{r}}\cdot(t^2\boldsymbol{r}-\boldsymbol{r}_0)+|t^2\boldsymbol{r}-\boldsymbol{r}_0|)\right] \quad (2.32)$$

where

$$t = \frac{a}{r}. \quad (2.33)$$

Setting $r = a$ in Equation (2.26) gives the Dirichlet data for the exterior problem

$$u^{+}(a\hat{\boldsymbol{r}}) = \frac{1}{\sigma}\boldsymbol{Q}\cdot\boldsymbol{\nabla}_{\boldsymbol{r}_0}\sum_{n=1}^{\infty}\sum_{m=-n}^{n}\frac{1}{n}\frac{{r_0}^n}{a^{n+1}}Y_n^m(\hat{\boldsymbol{r}}_0)^*Y_n^m(\hat{\boldsymbol{r}}) \quad (2.34)$$

Therefore, the exterior Dirichlet problem described in Equation (2.16)-(2.18) have the solution

$$u^{+}(\boldsymbol{r}) = \frac{1}{\sigma}\boldsymbol{Q}\cdot\boldsymbol{\nabla}_{\boldsymbol{r}_0}\sum_{n=1}^{\infty}\sum_{m=-n}^{n}\frac{1}{n}\frac{{r_0}^n}{r^{n+1}}Y_n^m(\hat{\boldsymbol{r}}_0)^*Y_n^m(\hat{\boldsymbol{r}}) \quad (2.35)$$

which can be expressed in Legendre polynomials using Laplace expansion in Equation (2.23)

$$u^{+}(\boldsymbol{r}) = \frac{1}{4\pi\sigma}\boldsymbol{Q}\cdot\boldsymbol{\nabla}_{\boldsymbol{r}_0}\sum_{n=1}^{\infty}\frac{2n+1}{n}\frac{{r_0}^n}{r^{n+1}}P_n(\hat{\boldsymbol{r}}\cdot\hat{\boldsymbol{r}}_0) \quad (2.36)$$

Using the same method, we can convert the series expression to a closed form solution.

$$u^{+}(\boldsymbol{r}) = \frac{1}{4\pi\sigma}\boldsymbol{Q}\cdot\boldsymbol{\nabla}_{\boldsymbol{r}_0}\sum_{n=1}^{\infty}(2+\frac{1}{n})\frac{{r_0}^n}{r^{n+1}}P_n(\hat{\boldsymbol{r}}\cdot\hat{\boldsymbol{r}}_0)$$

$$= \frac{1}{4\pi\sigma}\boldsymbol{Q}\cdot\boldsymbol{\nabla}_{\boldsymbol{r}_0}\left[\sum_{n=1}^{\infty}\frac{2{r_0}^n}{r^{n+1}}P_n(\hat{\boldsymbol{r}}\cdot\hat{\boldsymbol{r}}_0)+\sum_{n=1}^{\infty}\frac{1}{n}\frac{{r_0}^n}{r^{n+1}}P_n(\hat{\boldsymbol{r}}\cdot\hat{\boldsymbol{r}}_0)\right]$$

$$= \frac{1}{4\pi\sigma}\boldsymbol{Q}\cdot\boldsymbol{\nabla}_{\boldsymbol{r}_0}\left[\sum_{n=0}^{\infty}\frac{2{r_0}^n}{r^{n+1}}P_n(\hat{\boldsymbol{r}}\cdot\hat{\boldsymbol{r}}_0)-\frac{2}{r}P_0(\hat{\boldsymbol{r}}\cdot\hat{\boldsymbol{r}}_0)+\sum_{n=1}^{\infty}\frac{1}{n}\frac{{r_0}^n}{r^{n+1}}P_n(\hat{\boldsymbol{r}}\cdot\hat{\boldsymbol{r}}_0)\right]$$

$$= \frac{1}{4\pi\sigma}\boldsymbol{Q}\cdot\boldsymbol{\nabla}_{\boldsymbol{r}_0}\left[\frac{2}{|\boldsymbol{r}-\boldsymbol{r}_0|}-\frac{2}{r}+\frac{1}{r}\sum_{n=1}^{\infty}\frac{1}{n}\frac{{r_0}^n}{r^n}P_n(\hat{\boldsymbol{r}}\cdot\hat{\boldsymbol{r}}_0)\right]$$

$$= \frac{1}{4\pi\sigma}\boldsymbol{Q}\cdot\boldsymbol{\nabla}_{\boldsymbol{r}_0}\left[\frac{2}{|\boldsymbol{r}-\boldsymbol{r}_0|}-\frac{2}{r}-\frac{1}{r}ln\frac{1}{2}\left(1-\frac{r_0}{r}\hat{\boldsymbol{r}}\cdot\hat{\boldsymbol{r}}_0+\sqrt{1-2\frac{r_0}{r}\hat{\boldsymbol{r}}\cdot\hat{\boldsymbol{r}}_0+\frac{{r_0}^2}{r^2}}\right)\right]$$

$$= \frac{1}{4\pi\sigma}\boldsymbol{Q}\cdot\boldsymbol{\nabla}_{\boldsymbol{r}_0}\left[\frac{2}{|\boldsymbol{r}-\boldsymbol{r}_0|}-\frac{2}{r}-\frac{1}{r}ln\frac{1}{2r}(\hat{\boldsymbol{r}}\cdot(\boldsymbol{r}-\boldsymbol{r}_0)+|\boldsymbol{r}-\boldsymbol{r}_0|)\right] \quad (2.37)$$

For convenience, we define a function $F(\boldsymbol{r}, \boldsymbol{r}_0)$

$$F(\boldsymbol{r},\boldsymbol{r}_0) = r|\boldsymbol{r}-\boldsymbol{r}_0|^2+|\boldsymbol{r}-\boldsymbol{r}_0|\boldsymbol{r}\cdot(\boldsymbol{r}-\boldsymbol{r}_0). \quad (2.38)$$

Then Equation (2.37) reduces to

$$u^+(\boldsymbol{r}) = \frac{1}{4\pi\sigma}\boldsymbol{Q}\cdot\boldsymbol{\nabla}_{\boldsymbol{r}_0}\left[\frac{2}{|\boldsymbol{r}-\boldsymbol{r}_0|}-\frac{2}{r}-\frac{1}{r}ln\frac{F(\boldsymbol{r},\boldsymbol{r}_0)}{2r^2|\boldsymbol{r}-\boldsymbol{r}_0|}\right]. \quad (2.39)$$

Perform the gradient operation we arrive at

$$u^+(\boldsymbol{r}) = \frac{1}{4\pi\sigma}\boldsymbol{Q}\cdot\left[\frac{2(\boldsymbol{r}-\boldsymbol{r}_0)}{|\boldsymbol{r}-\boldsymbol{r}_0|^3}+\frac{|\boldsymbol{r}-\boldsymbol{r}_0|\hat{\boldsymbol{r}}+(\boldsymbol{r}-\boldsymbol{r}_0)}{F(\boldsymbol{r},\boldsymbol{r}_0)}\right]. \quad (2.40)$$

The analytical solution of electric potential outside a conductive sphere, which was reported in [11, 12], provides a solid fundamental theoretical basis for our simulation and experimental studies.

# 3.0 SIMULATION

We have shown that the spherical volume conductor model has a closed form solution either inside or outside the conductor, which is obtained by solving the Laplace equations under the boundary conditions. The exterior electric potential provides theoretical support for the non-contact ECG measurement. However, since a current dipole is an ideal concept, people cannot directly investigate the application of the spherical volume conductor model. Nevertheless, the current dipole can be simulated by a real model. In this chapter, we propose a model and use the simulation tools to demonstrate the feasibility of the model. Instead of solving the Laplace equations under the boundary conditions, the forward problem is solved using finite element method (FEM) to numerically compute the electric potential. Then, the computed and theoretical potentials are compared.

## 3.1 THEORETICAL SOLUTION OF ELECTRIC POTENTIAL

We consider the simplest case, that is, the current dipole locates at the center of the conducting sphere. Due to the symmetric property, we assume that the moment of the dipole is along the $+z$ direction, shown in Figure 4. In the ECG study, we only consider the electric potential on the surface of the sphere since electrodes will be directly attached on the skin of our human body to measure the electric signals.

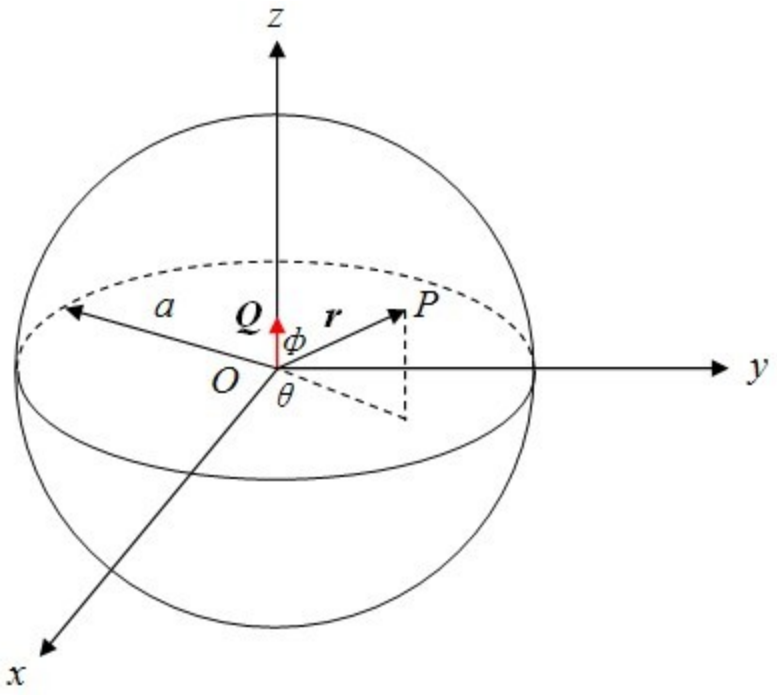


**Figure 4.** The current dipole locates at the center of the sphere.

For any point *P* on the surface of the sphere, we can use Equation (2.40) to calculate the electric potential.

$$u(a\hat{\boldsymbol{r}}) = \frac{1}{4\pi\sigma}\boldsymbol{Q}\cdot\left[\frac{2(\boldsymbol{r}-\boldsymbol{r}_0)}{|\boldsymbol{r}-\boldsymbol{r}_0|^3}+\frac{|\boldsymbol{r}-\boldsymbol{r}_0|\hat{\boldsymbol{r}}+(\boldsymbol{r}-\boldsymbol{r}_0)}{F(\boldsymbol{r},\boldsymbol{r}_0)}\right]$$

$$= \frac{1}{4\pi\sigma}\boldsymbol{Q}\cdot\left[\frac{2\boldsymbol{r}}{|\boldsymbol{r}|^3}+\frac{|\boldsymbol{r}|\hat{\boldsymbol{r}}+\boldsymbol{r}}{F(\boldsymbol{r},\boldsymbol{0})}\right] \tag{2.41}$$

where using Equation (2.38),

$$F(\boldsymbol{r},\boldsymbol{0}) = r|\boldsymbol{r}|^2 + |\boldsymbol{r}|\boldsymbol{r}\cdot\boldsymbol{r} = 2|\boldsymbol{r}|^3. \tag{2.42}$$

Then Equation (2.41) turns to

$$u(a\hat{\boldsymbol{r}}) = \frac{1}{4\pi\sigma}\boldsymbol{Q}\cdot\left[\frac{2\boldsymbol{r}}{|\boldsymbol{r}|^3}+\frac{|\boldsymbol{r}|\hat{\boldsymbol{r}}+\boldsymbol{r}}{F(\boldsymbol{r},\boldsymbol{0})}\right] = \frac{1}{4\pi\sigma}\boldsymbol{Q}\cdot\left[\frac{2\boldsymbol{r}}{|\boldsymbol{r}|^3}+\frac{|\boldsymbol{r}|\hat{\boldsymbol{r}}+\boldsymbol{r}}{2|\boldsymbol{r}|^3}\right]$$

$$= \frac{3}{4\pi\sigma a^2}\boldsymbol{Q}\cdot\hat{\boldsymbol{r}} = \frac{3}{4\pi\sigma a^2}Qcos\phi. \tag{2.43}$$

For spherical coordinates, $\Phi$ varies from 0 to $2\pi$. As a point moving from the north pole to the south pole of the sphere, the electric potential monotonically decreases from the most positive

value to the most negative value. The potential at the equator equals zero. The points at the same latitude have the same electric potential. Since the potential is a scalar, we can use the color map to indicate the potential distribution on the surface of the sphere, shown in Figure 5.

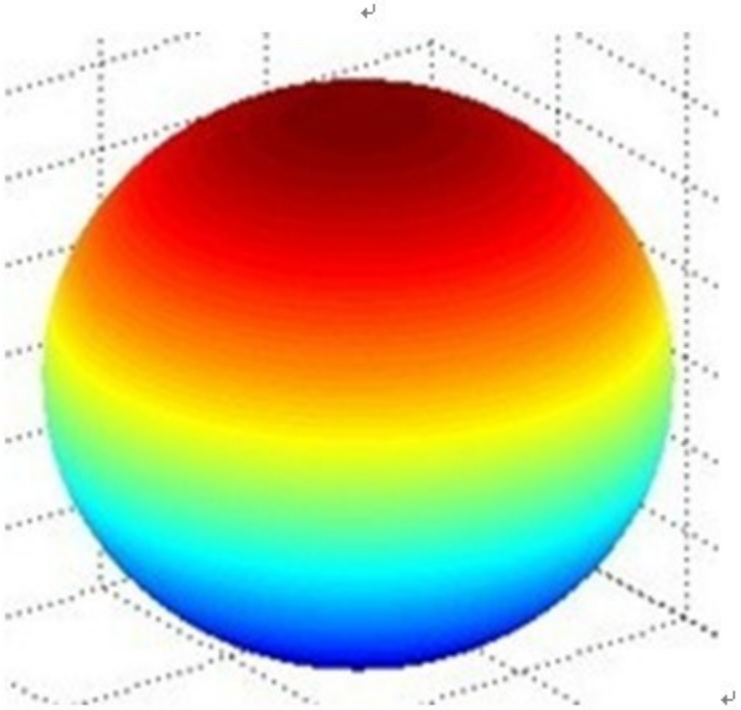

**Figure 5.** The electric potential on the surface of the sphere when the current dipole locates at the center of the sphere

### 3.2 THE ELECTRIC POTENTIAL SIMULATED BY ANSOFT MAXWELL 12

The simulation tool we used is Ansoft Maxwell 12, which requires us to define mesh on built model and will numerically compute the electric field using the finite element method based on the pre-defined excitations and boundary conditions.

Due to the symmetry, the simulation can be performed in 2D mode. Hence, the conducting sphere can be represented by a circle with a conductivity 1/222 $cm^{-1} \cdot \Omega^{-1}$, which is the value for soft tissues [14].

The current dipole is an ideal concept, which assumes the primary current originates from a single point and returns to this point after traveling a closed loop in the conducting medium. Figure 6 illustrates the current dipole, where the arrows indicate the direction of the primary current.

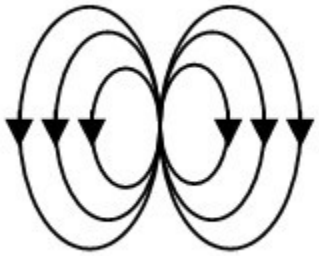

**Figure 6.** The current dipole model

However, this ideal model cannot be constructed directly using Ansoft Maxwell 12. A physical model with a similar behavior is needed to substitute the current dipole model. An idea is to build a pair of metal electrodes separated by an insulator, shown in Figure 7. To simplify the model, the two electrodes and the central insulator have cylindrical shapes. The whole model is placed at the center of the conducting sphere. We add positive and negative voltage excitations on the two electrodes respectively. The center insulator is hard to conduct electricity, while the surrounding medium has a conductivity of 1/222 $cm^{-1} \cdot \Omega^{-1}$. Hence, the current is generated and traveling from the positive electrode to the negative electrode, exhibiting the same phenomenon describe in Figure 6.


**Figure 7.** A physical model to substitute the current dipole

Specifically, the diameter of the conducting sphere is 8 in, which is much larger than the size of the electrodes and the insulator. Hopefully, the electric potential on the surface of the sphere is supposed to have no difference from that caused by a current dipole at the center of the sphere. The excitations applied across the electrodes are $\pm 5$V, zero initial phase, 60 Hz sinusoidal signals.

After simulation, the primary current density is plotted in Figure 8. The arrow indicates the direction of the local primary current density, while the color tells the magnitude of the current density. Intuitively, the primary current produced by this model is quite similar to what we defined for the current dipole in Figure 6.

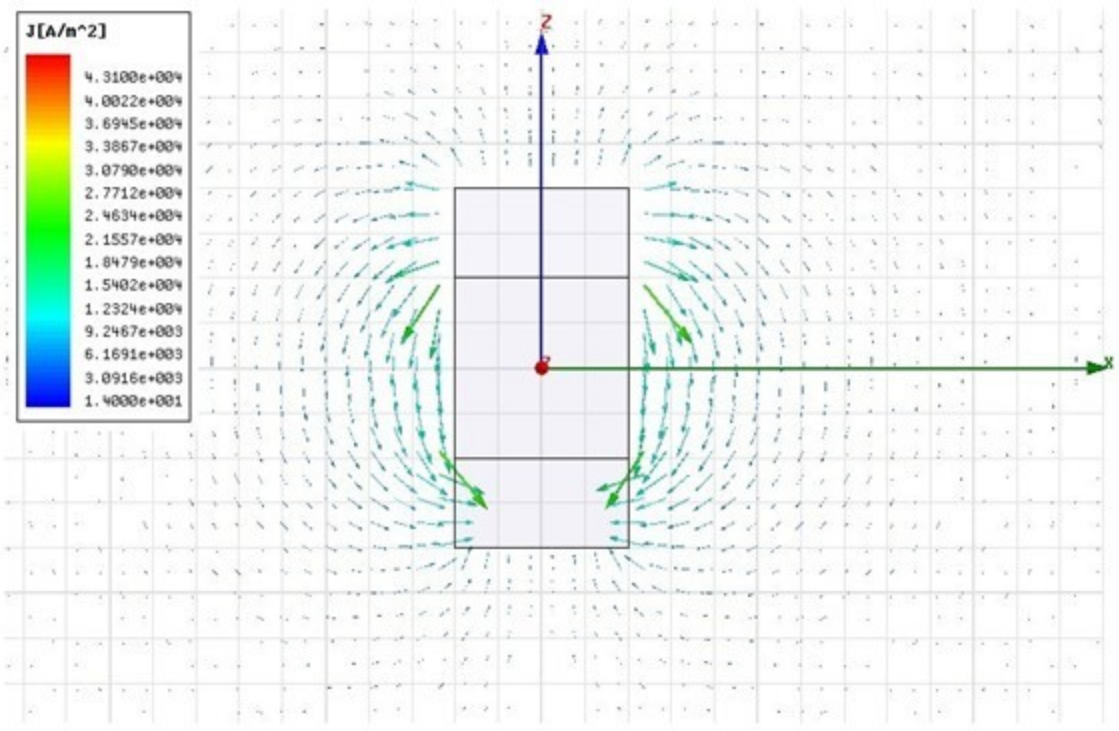


**Figure 8.** The plot of primary current density around the dipole.

To better demonstrate the feasibility of using this model to simulate the ideal current dipole, the electric potential is plotted in Figure 9.

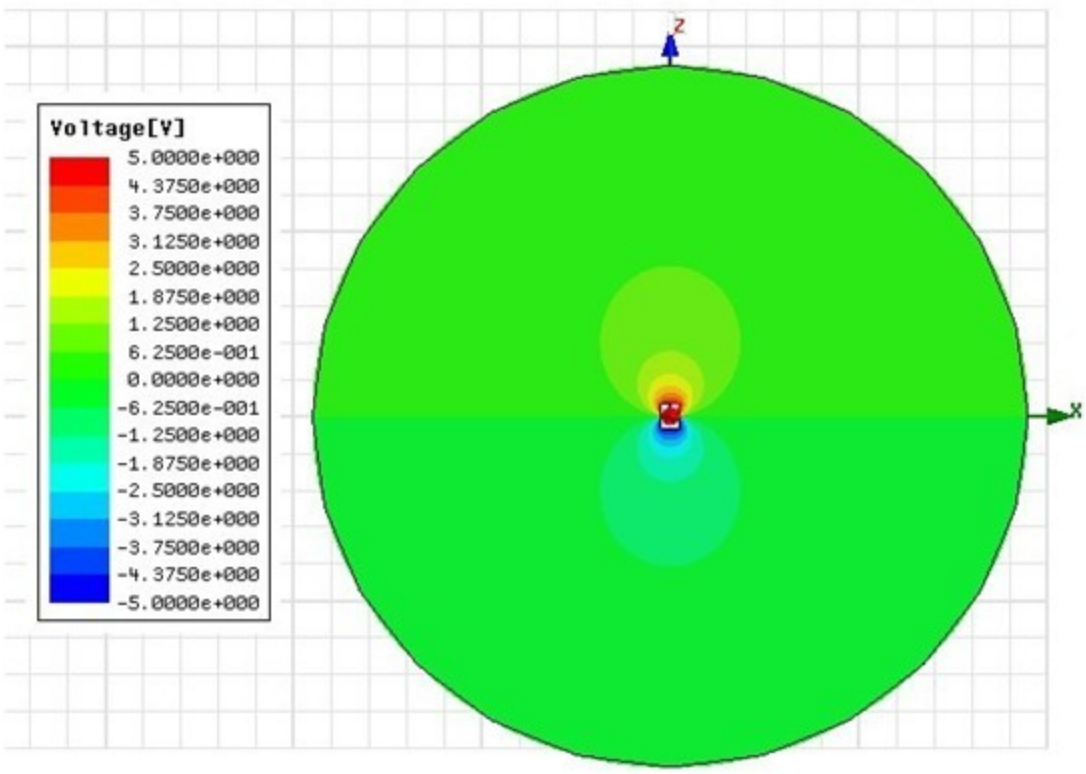


**Figure 9.** The plot of electric potential inside and on the surface of the sphere

The magnitude of the electric potential can be indicated using different colors since the potential is a scalar. For the areas near the two electrodes, the potential is close to $\pm 5$V, which can be illustrated by either red or blue color. For the area far from the electrodes, the value of potential is small and close to 0, which can be indicated using green color.

It is difficult to recognize the distribution of electric potential on the surface of the sphere directly from the color map in Figure 9. However, the potential values at each point can be exported, which enables us to find out the relation between the electric potential and the location on the surface of the sphere, shown in Figure 10. As a point on the surface travels clockwise from the north pole and returns to the start point, the potential approximately exhibits a cosine-like relation on the angle $\Phi$.

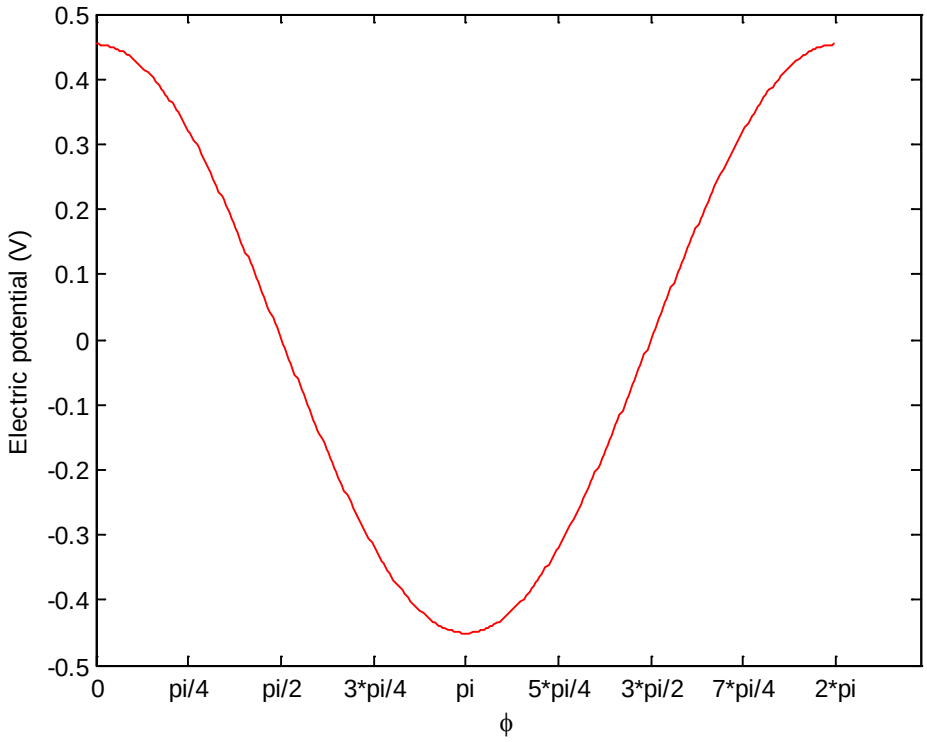


**Figure 10.** The plot of electric potential on the surface of the sphere v. s. the angle $\Phi$

For the physical model constructed in the Maxwell software, the dipole moment $Q$ cannot be directly estimated. Nevertheless, we will be able to compare the simulated result with the theoretical calculation through normalization. At the north pole, the simulated electric potential gives the maximum value 0.4535 V. Therefore, we compare the simulated result with 0.4535*cos($\Phi$) to investigate the errors of the simulation, illustrated in Figure 11.

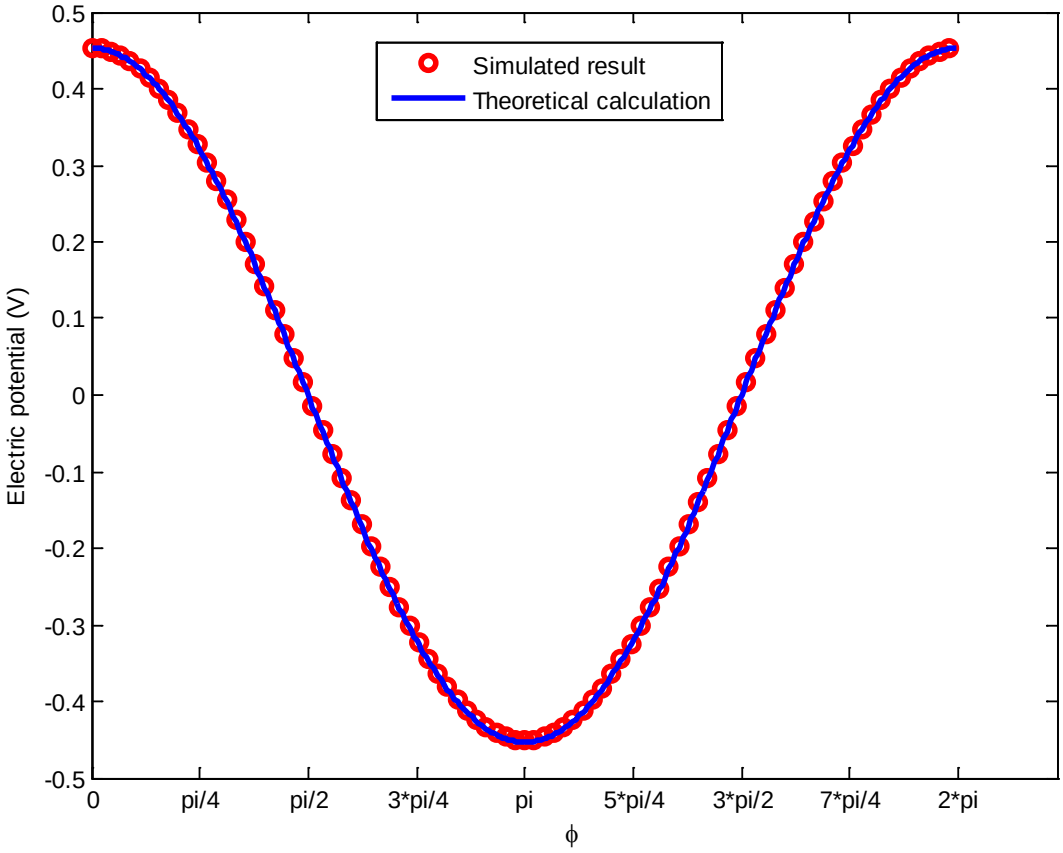


**Figure 11.** A comparison between the simulated potential and the theoretical calculation

After normalization, the two curves almost coincide, implying the designed model produces the same electric potential on the surface of the sphere as the theoretical conclusion using the spherical volume conductor model. Since this model generates similar primary current and electric potential on the surface of the sphere, we will be able to use this model to implement experimental investigation on ECG electrodes design.

# 4.0 EXPERIMENTAL DESIGN AND RESULTS

This section describes the experimental design and the results. Section 4.1 discusses the design of capacitive electrodes and the construction of the spherical volume conductor model. Section 4.2 demonstrates that our capacitive electrodes can realize both direct and non-contact measurement of electric potentials from the spherical volume conductor model. Section 4.3 investigates the location that provides most significant signals. Finally, Section 4.4 shows the results of measure real ECG signals from the chest.

## 4.1 EXPERIMENTAL DESIGN

### 4.1.1 Spherical volume conductor model

The spherical volume conductor model consists of a conducting sphere and an interior current dipole. The conducting sphere is constructed by filling a hollow latex ball with salted water. The diameter of the sphere is 8 in, while the conductivity of the salted water is controlled to 1/222 $\Omega^{-1} \cdot cm^{-1}$, similar to the average conductivity value of the biological tissue of our human body.

In previous section, we use the simulation tool to verify that a current dipole can be modeled as two small metal electrodes separated by an insulator. In the experimental design, we use the X-antenna similar to the model described in [15] to represent the current dipole, shown in

Figure 12. It consists of a source and a sink separated by a small distance. Once the antenna dipole is immersed in salted water and excited by an AC signal, the current travels from the source to the sink, exhibiting the behavior of a current dipole.

**Figure 12.** Actual construction of the antenna dipole.

### 4.1.2 Electrodes to measure the signal

Capacitive electrodes can be designed to measure the surface potential of the conducting sphere. Figure 13 is the physical view of our electrode. This copper electrode consists of one large reference and two circular electrodes. The diameters of the large reference electrode and the small sensing electrode are 7 cm and 1.5 cm, respectively. The two sensing electrodes are separated by 4 cm. When applying this new type of electrodes to the spherical volume conductor model, the contact between the metal electrodes and the latex surface of the sphere is not ohmic. Intuitively, this electrode will not be able to sense the potential on the surface of the sphere. However, the measuring part behaves like a parallel plate capacitor since the copper electrode

and the inside conducting salted water form two conducting layers, while the latex shell, air space and the cloths form the dielectric layer of the capacitor. Because the dipole antenna is excited by AC signals, the electric potential is generated on the one side of the capacitor, which enables the capacitor to keep charging and discharging. Hence, the capacitive electrodes are able to measure the electrical signals on the surface of the sphere through capacitive coupling effect. Since the reference electrode is large, it senses the average of the potential distribution within the area of its coverage when placed on the top of the chest, which provides stable, grounded reference, reducing the common noise. The smaller electrodes, located within the two circular holes of the reference electrode, reflect the local potentials of the heart. Besides, the far distance between two sensing electrodes will help to avoid interference. Moreover, the thin-film design of these electrodes yields very small capacitance between sensing electrodes and the reference electrode, which helps to avoid signal leakage during the measurement. In addition, the wires connected to the three metal electrodes were twisted together, which further can help to reduce the noise.

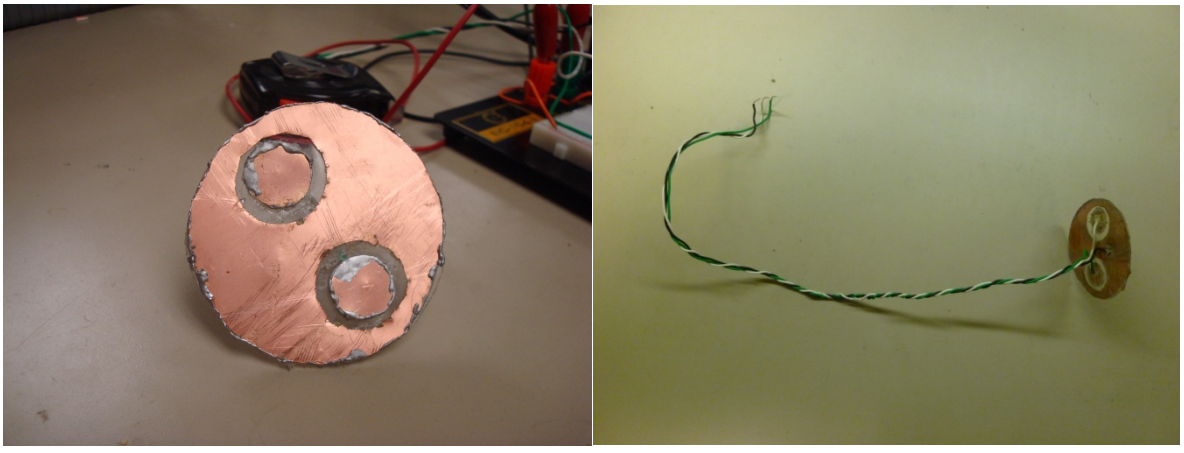

**Figure 13.** The capacitive electrode used in the experiment.

### 4.1.3 Experimental setup

Figure 14 shows the design of the experiment. The dipole antenna is excited by an AC signal generated by a function generator. The capacitive electrodes are used to capture the electric potential on the surface of the sphere. Since the value of the surface potential is very small, a differential amplifier is applied before comparing the detected signal with the original signal in an oscilloscope. The differential amplifier we used is the Texas Instruments INA118 instrumentation amplifier with input impedance as high as 10 GΩ. The gain of the amplifier is set to be 200 in our experiment. In addition, the common mode rejection ratio is 120 dB for signals with frequencies less than 100 Hz, which is good enough reject the input signals common to both input leads.

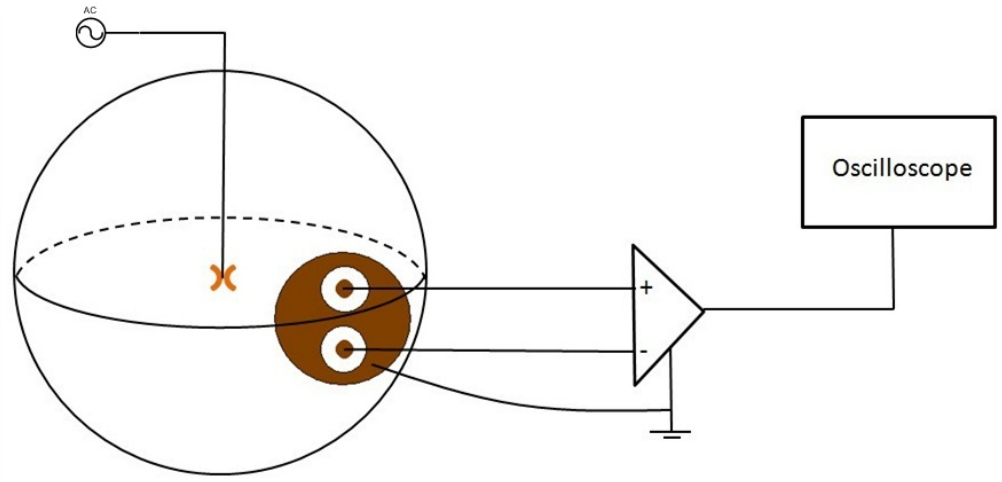


(a)

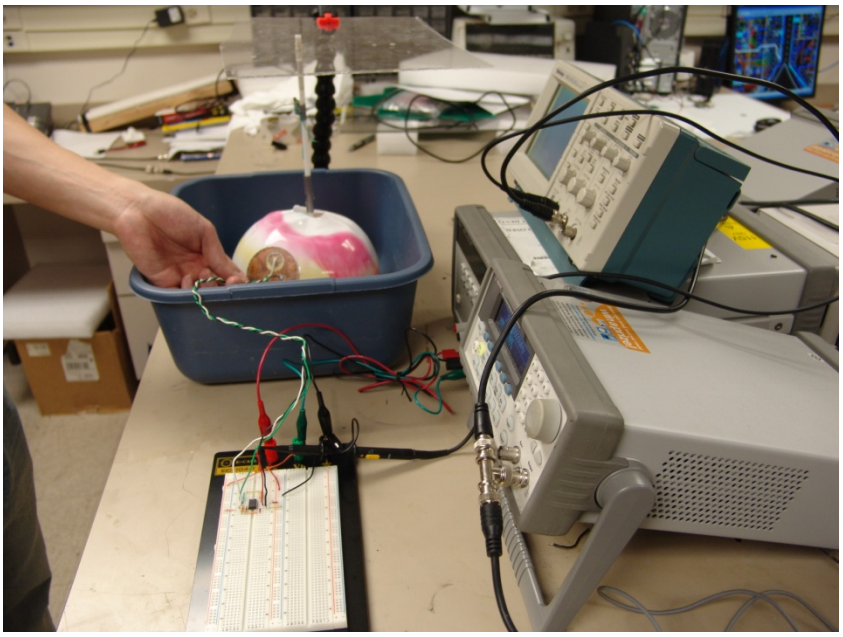

(b)

**Figure 14.** (a) Experimental design. (b) Actual setup of the experiment

## 4.2 MEASURING SIGNALS USING CAPACITIVE ELECTRODES

An experiment was performed to verify whether the capacitive electrodes can measure signals from the surface of the sphere when the dipole is excited by AC signals. Typically, the default bandwidth of 12-lead ECG data is 0.05 to 150 Hz. Therefore, the frequency of sinusoid signals and ECG signals we applied on the dipole is 50 Hz, while the peak-to-peak value of the signals is 4 V. We also tried the non-contact measurement by wrapping the electrodes with several layers of cloths. Figure 15, below, shows the captured signals at the same position in different cases.

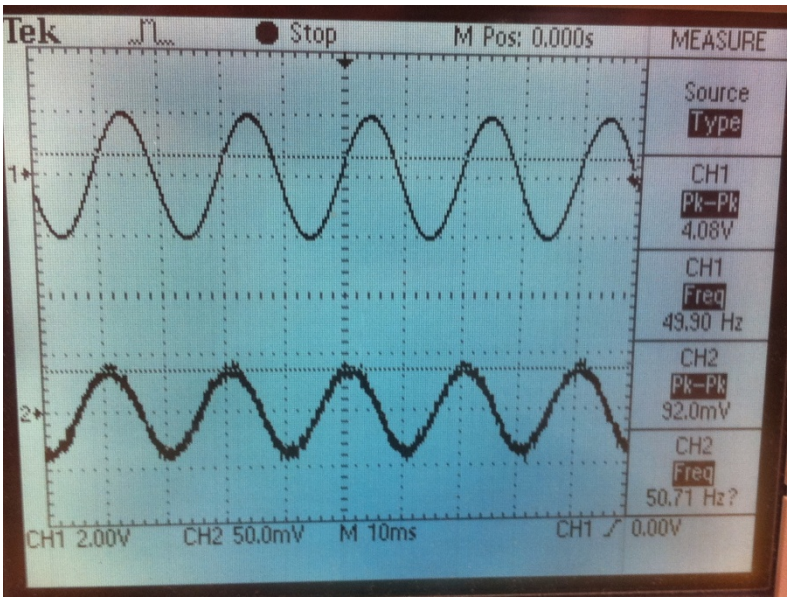
Tek
Stop
M Pos: 0.000s
MEASURE
Source
Type
CH1
Pk-Pk
4.08V
CH1
Freq
49.90 Hz
CH2
Pk-Pk
92.0mV
CH2
Freq
50.71 Hz?
CH1 2.00V
CH2 50.0mV
M 10ms
CH1 ∕ 0.00V

(a)

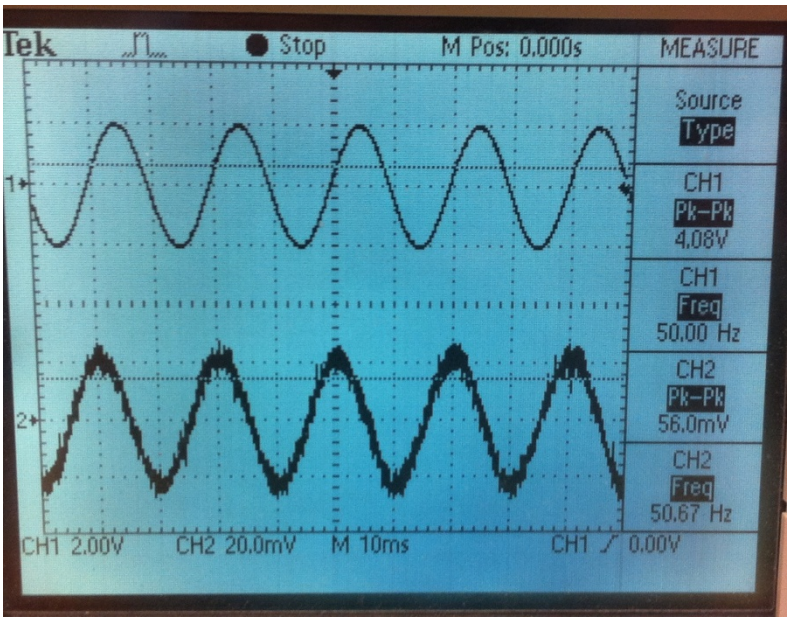
Tek
Stop
M Pos: 0.000s
MEASURE
Source
Type
CH1
Pk-Pk
4.08V
CH1
Freq
50.00 Hz
CH2
Pk-Pk
56.0mV
CH2
Freq
50.67 Hz
CH1 2.00V
CH2 20.0mV
M 10ms
CH1 ∕ 0.00V

(b)

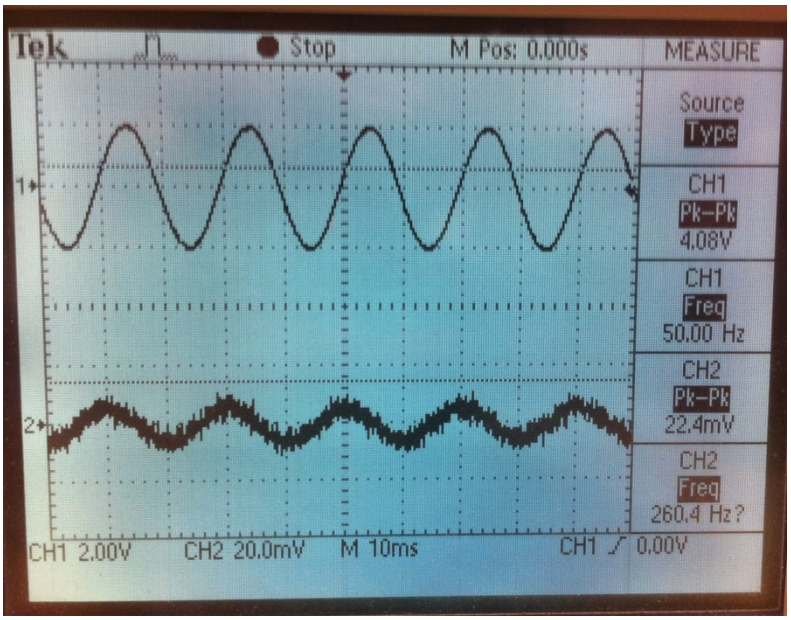


(c)

**Figure 15.** Measuring the surface potential when the X-dipole antenna is excited by a sinusoid signal of 50 Hz: (a) Directly attaching the electrodes to the surface of the sphere. (b) Wrapping the electrodes by one layer of cloths. (c) Wrap the electrodes by two layers of cloths.

In the above figures, the top curve is the applied sinusoid signals, and the bottom one is the measurement from the capacitive electrodes in different cases. Compared with the input sinusoid signal, the detected signals have the same frequency. This can be explained by Equation (2.43) since the surface potential is proportional to the excitation source. The introduced layers of cloths reduce the peak-to-peak values of the detected signals and generate more noises. Nevertheless, capacitive electrodes are able to realize the non-contact measurement, which is favorable in real-time heart signal monitoring.

Same conclusions can be drawn for cardiac excitations (peak-to-peak value: 3 V, frequency: 60 Hz). Figure 16 shows the results when a cardiac signal is applied to the dipole antenna.

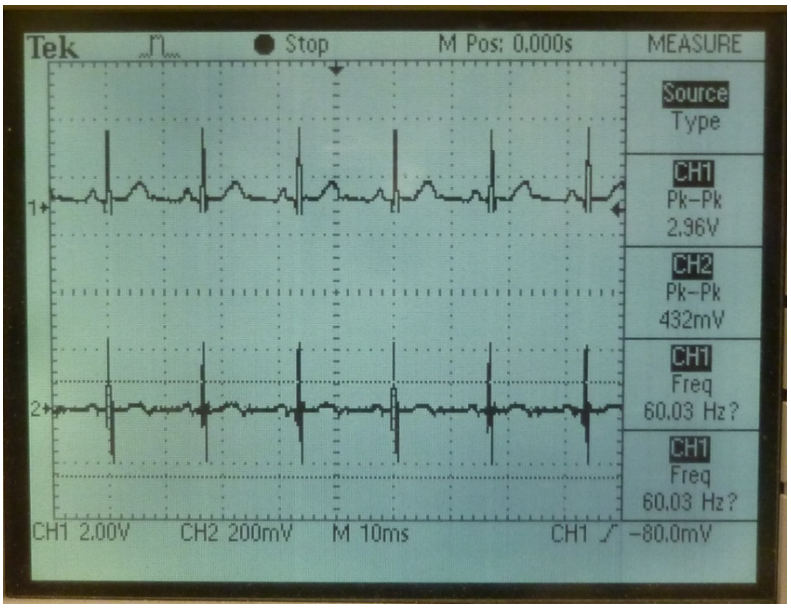
Tek
Stop
M Pos: 0.000s
MEASURE
Source
Type
CH1
Pk-Pk
2.96V
CH2
Pk-Pk
432mV
CH1
Freq
60.03 Hz?
CH1
Freq
60.03 Hz?
CH1 2.00V
CH2 200mV
M 10ms
CH1 ⁄
-80.0mV

(a)


Tek
Stop
M Pos: 0.000s
MEASURE
Source
Type
CH1
Pk-Pk
3.04V
CH2
Pk-Pk
140mV
CH1
Freq
59.95 Hz?
CH1
Freq
59.95 Hz?
CH1 2.00V
CH2 100mV
M 10ms
CH1 ⁄
-80.0mV

(b)

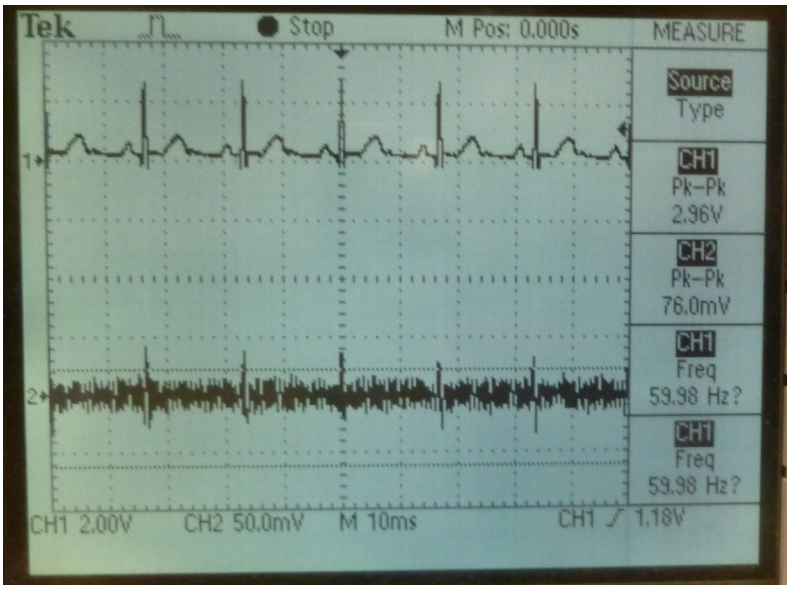


(c)

**Figure 16.** Measuring the surface potential when the dipole antenna is excited by a cardiac signal. (a) Directly attaching the electrodes to the surface of the sphere. (b) Wrapping the electrodes by one layer of cloth. (c) Wrap the electrodes by two layers of cloths.

## 4.3 MEASURING ELECTRIC POTENTIAL AT DIFFERENT LOCATIONS

The measured signals actually tell the potential difference between the two sensing electrodes. Since the potential is location-dependent and the distance between the two sensing electrodes is fixed, we should detect different signals when the electrodes are placed at different positions or with different orientations. In this section, we combine the theoretical analysis and the experimental implementation for the purpose of finding the best location and orientation which can yield an output signal with most significant peak-to-peak value.

For the current dipole with a moment pointing to the +$z$ direction locates at the origin, Equation (2.43) indicates the potential of a certain point on the sphere is proportional to the cosine value of $\Phi$, the angle between the +$z$ and the location vector $\boldsymbol{r}$. In other words, the potential of one point in the sphere surface is determined by the latitude of this point.

We define $\Phi_1$ and $\Phi_2$ for the two sensing electrodes and assume $\Phi_1$ is fixed while $\Phi_2$ is variant. That is, we fix the position of one electrode and move the second one to change the orientation of the whole electrodes. Since the geometry of the electrodes is much smaller than that of the sphere, the difference between $\Phi_1$ and $\Phi_2$ is relatively small as we move the second sensing electrode. In order to obtain the maximum potential difference between the two sensing electrodes, or the largest difference between $cos\Phi_1$ and $cos\Phi_2$, we need to find the maximum value of $|\phi_1 - \phi_2|$. Suppose the first sensing electrode is fixed on the point $P_1$, shown in Figure 17. Because the distance between the two sensing electrodes is invariant, we have the largest difference between $\Phi_1$ and $\Phi_2$ when the two sensing electrodes are aligned on the same longitude.

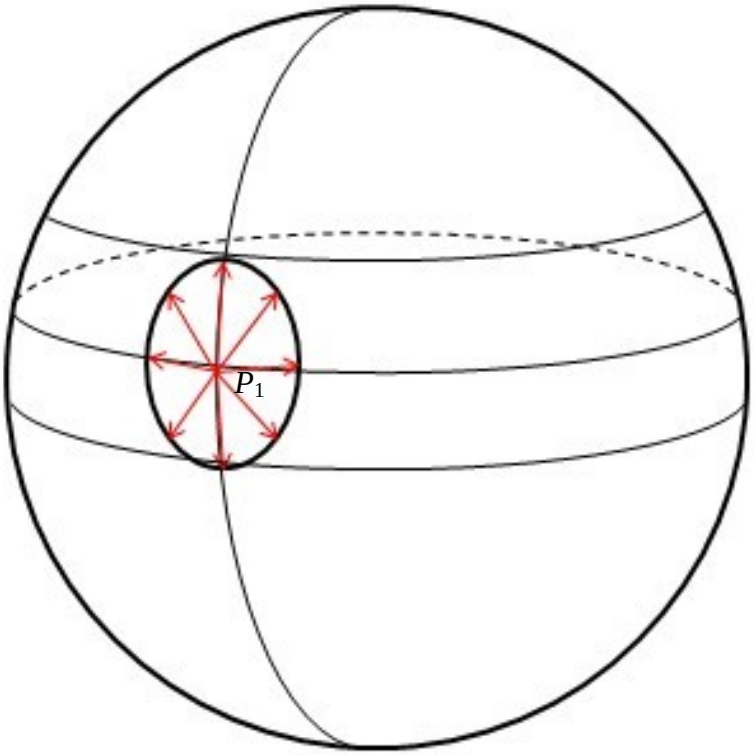


**Figure 17.** Two sensing electrodes aligned on the same longitude gives the maximum difference of the latitude.

Since the model is symmetric, the measured result will not be affected by which longitude we are using to place the electrodes. Experiment is performed to verify this symmetric property. The testing strategy is explained in Figure 18. Instead of pointing to the +*z* direction, the moment vector in our experiment is on the horizontal plane because of the actual construction of the dipole antenna, shown in Figure 12. Suppose the dipole moment is pointing to the inside of the paper, then we maintained $\Phi_1$ and $\Phi_2$ constant with respect to the new dipole moment direction and tried several equivalent longitudes of the new model. For simplicity, the two sensing electrodes, depicted as orange dots in the figure, are symmetric across the equivalent equator. Six different positions of the electrodes are labeled from "*1*" to "*6*" in Figure 18. The intersection angle between plane $P_2$ and the horizontal plane, $P_1$, is $45^\circ$, while the angle between $P_3$ and $P_1$ is $135^\circ$.

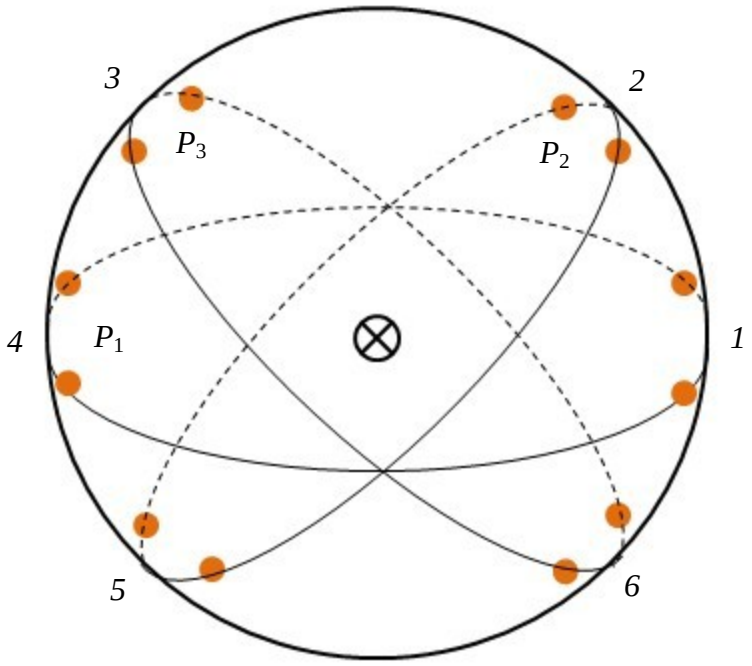


**Figure 18.** Measure the signals from six different locations around the equivalent equator.

A sinusoid signal with a frequency of 50 Hz and a peak-to-peak value of 2 V is applied on the dipole antenna. Table 1, below, lists the measured results at the six labeled locations.

**Table 1.** Measured results from six labeled positions

| | 1st Measurement (mV) | 2nd Measurement (mV) | 3rd Measurement (mV) | 4th Measurement (mV) | Mean Value (mV) |
|---|---|---|---|---|---|
| Position 1 | 176 | 182 | 180 | 174 | 178 |
| Position 2 | 170 | 168 | 168 | 176 | 170.5 |
| Position 3 | 172 | 176 | 162 | 170 | 170 |
| Position 4 | 180 | 166 | 176 | 168 | 172.5 |
| Position 5 | 172 | 164 | 170 | 172 | 169.5 |
| Position 6 | 168 | 174 | 170 | 164 | 169 |

The mean value and standard deviation of the average peak-to-peak values of the captured signals in the six positions are 171.58 mV and 3.07 mV. The standard deviation is very small compared to the mean value of the average peak-to-peak values of the detected signals. Therefore, once the two sensing electrodes have fixed angles $\Phi_1$ and $\Phi_2$ with respect to the dipole moment direction, the measured signal will not related to the equivalent longitude on which they are placed.

It has been proven that signals with maximum peak-to-peak values only can be captured when both sensing electrodes are aligned on an arbitrary equivalent longitude. Further investigation is needed to find the actual positions on the corresponding longitude. Since the two sensing electrodes are on the same longitude, the difference between $\Phi_1$ and $\Phi_2$, $\Delta\phi = \phi_1 - \phi_2$, is constant. The maximum $|u(\phi_1) - u(\phi_2)|$ occurs when the derivative of $u(\phi)$ has largest absolute value. Take the derivative of $u(\phi)$ in Equation (2.43), we have

$$u'(\phi) = -\frac{3}{4\pi\sigma a^2} Q sin\phi. \tag{4.1}$$

For $\phi \in [0,2\pi]$, $u'(\phi) = 0$ when $\phi = 0, \pi, 2\pi$; $|u'(\phi)| = 1$ when $\phi = \frac{\pi}{2}, \frac{3\pi}{2}$. Therefore, we should detect the signals with minimum peak-to-peak value at the points corresponding to $\phi = 0, \pi, 2\pi$ and obtain the signals with maximum peak-to-peak value at the points corresponding to $\phi = \frac{\pi}{2}, \frac{3\pi}{2}$. Another experiment was implemented to find the signals with maximum peak-to-peak values. In the big circle on the surface of the sphere shown in Figure 19, eight different locations representing $\phi = 0, \frac{\pi}{4}, \frac{\pi}{2}, \frac{3\pi}{4}, \pi, \frac{5\pi}{4}, \frac{3\pi}{2}, \frac{7\pi}{4}$ is labeled as Position "*a*" through "*h*" respectively. The excitation applied on the dipole antenna was a sinusoid signal with a frequency of 50 Hz and a peak-to-peak value of 2 V. Table 2 lists the peak-to-peak values of the measured signals from the eight positions.

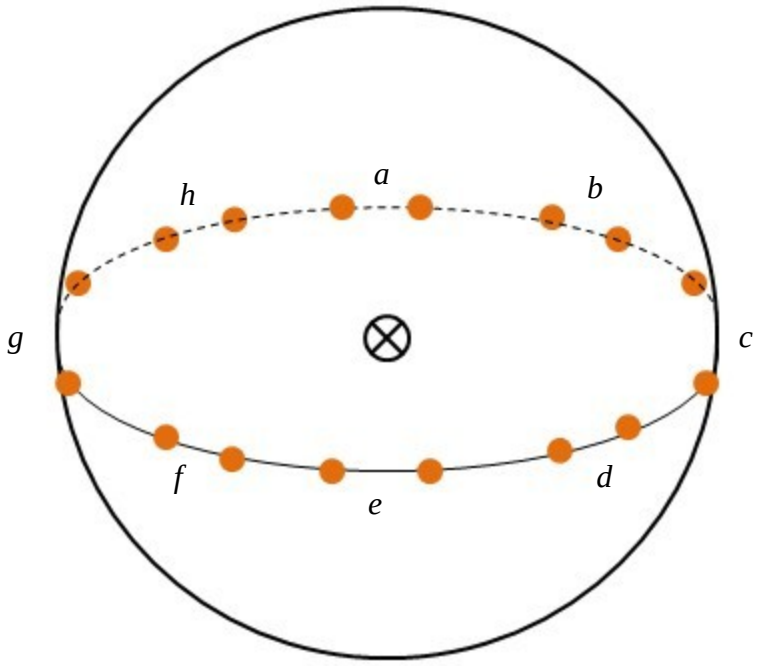


**Figure 19.** Measure the signals from eight different locations around the equivalent longitude.

**Table 2.** Measured results from eight labeled positions

| | 1st Measurement (mV) | 2nd Measurement (mV) | 3rd Measurement (mV) | 4th Measurement (mV) | Mean Value (mV) |
|---|---|---|---|---|---|
| Position *a* | 60 | 76 | 62 | 54 | 63 |
| Position *b* | 112 | 136 | 112 | 128 | 122 |
| Position *c* | 176 | 180 | 180 | 174 | 177.5 |
| Position *d* | 112 | 120 | 128 | 132 | 123 |
| Position *e* | 80 | 60 | 74 | 68 | 70.5 |
| Position *f* | 124 | 108 | 120 | 110 | 115.5 |
| Position *g* | 180 | 164 | 176 | 168 | 172 |
| Position *h* | 120 | 112 | 116 | 122 | 117.5 |

At Position *a* and *e*, where $\phi = 0, \pi$, we can measure the weakest signals. This is reasonable since the two sensing electrodes are on the same latitude and sense the same electric potential when $\phi = 0, \pi$. On the other hand, Position *c* and *g*, where $\phi = \frac{\pi}{2}, \frac{3\pi}{2}$, provide much stronger signals. Therefore, when the two sensing electrodes are placed on the same longitude and on the position where $\phi = 0, \pi$ with respect to the dipole moment, we can capture the strongest signals using the capacitive electrodes. In other words, as long as the line connecting the two electrodes is parallel to the direction of the dipole moment, the capacitive electrodes are able to measure the most significant signals.

## 4.4 MEASURING REAL ECG SINGALS

We have theoretically analyzed, simulated, and experimentally implemented the application of using capacitive electrodes to measure ECG signals based on the spherical volume conductor model. In this section, the constructed electrodes are shown to monitor the real heart activity.

Theoretically, the current dipole keeps moving and rotating inside the heart, which reflects different body surface potentials and ECG signals, as shown in Figure 20 [16]. The strongest R wave will be detected when the dipole is in diagonal position. In the view of body surface potential mapping, EKG++ Demo (EZCardio Software) indicates the diagonal regions provide very large potential difference when the dipole is in the diagonal position, as displayed in Figure 21.

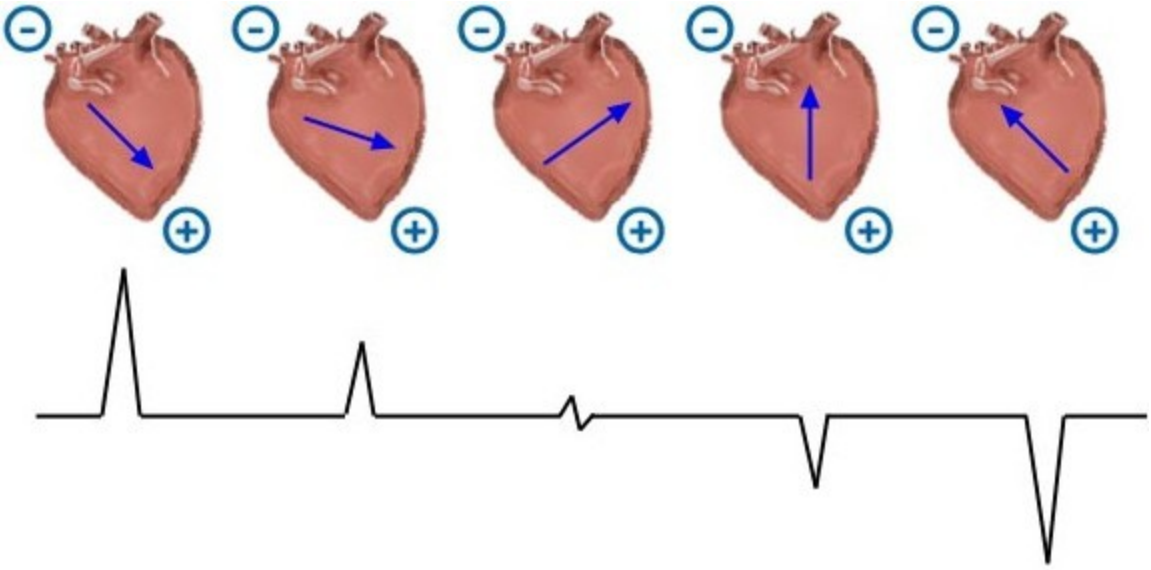

**Figure 20.** Different ECG waveforms yielded by rotating current dipole.

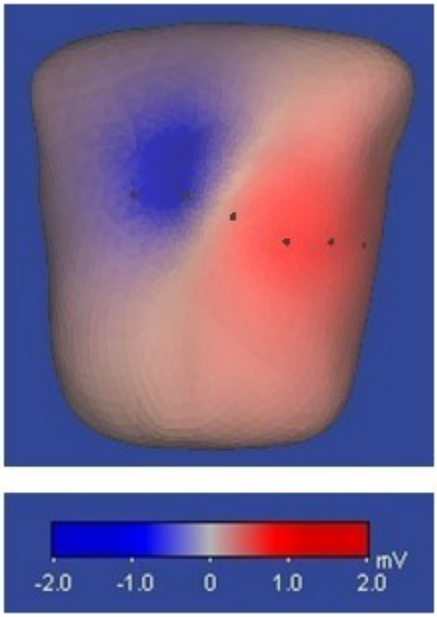


**Figure 21.** Body surface potential mapping when the dipole is in diagonal position.

During the experiment, we tried different orientations and found that the best orientation for a neat ECG output is diagonal across the heart, as shown in Figure 22, which matches the theoretical analysis. Figure 23 shows an example of an ECG output without much concern with the orientation of the electrodes. In this case, the electrodes were not placed diagonal across the

heart but more horizontally. As we place the electrodes diagonal across the heart, a neat ECG signal was captured, shown in Figure 24.

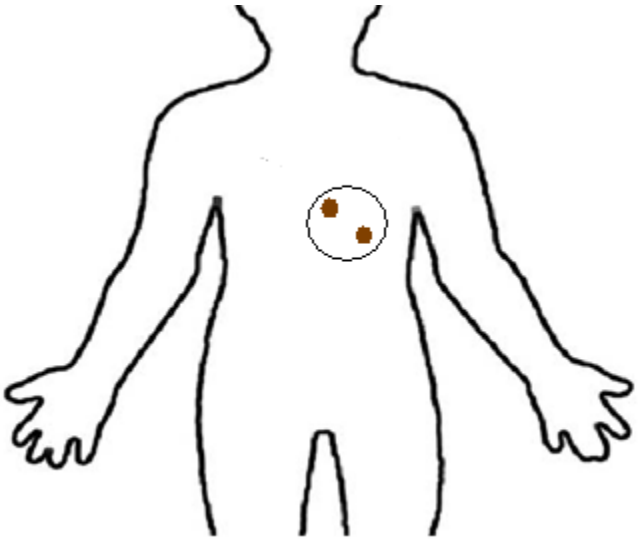

**Figure 22.** Orientation of capacitive electrodes for best ECG output.

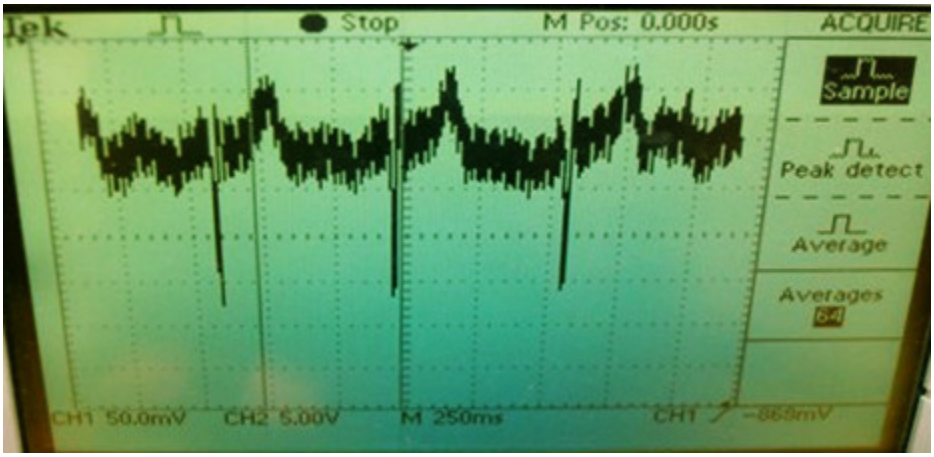


**Figure 23.** Noisy ECG output captured from horizontally placed electrodes.

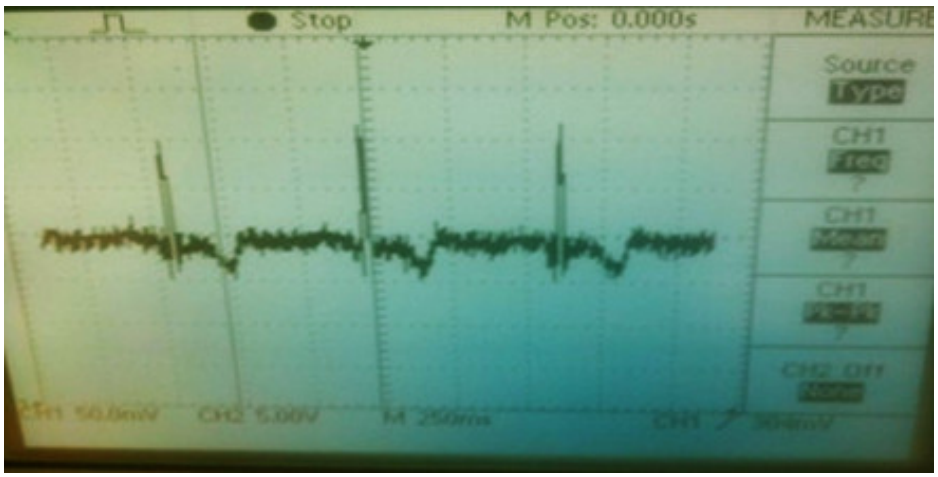


**Figure 24.** Neat ECG output captured from diagonally placed electrodes.

The capacitive electrodes have been demonstrated to realize non-contact measurement on spherical volume conductor model. For the real-time heart monitoring, the electrodes can also measure the ECG output from the cloth layer. Figure 25, below, shows the results of direct measurement, measuring from one layer of cloth, and from two layers of cloth, respectively. As more layers of cloth are introduced, the ECG output will become noisier.

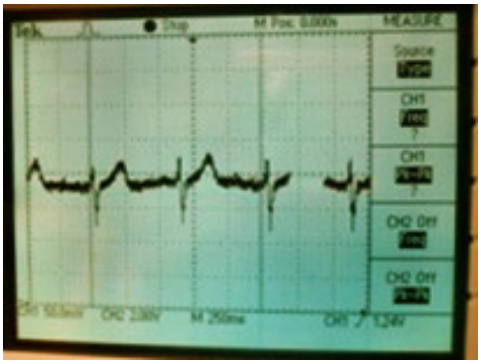

(a)

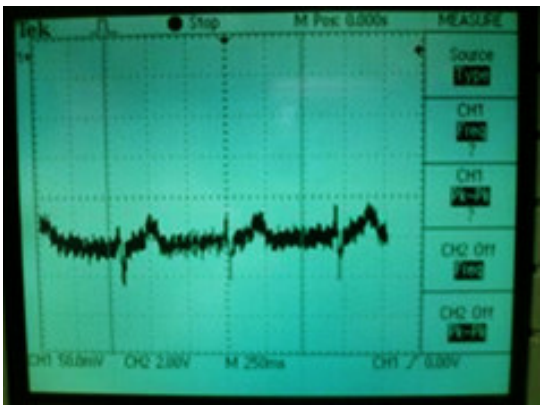


(b)

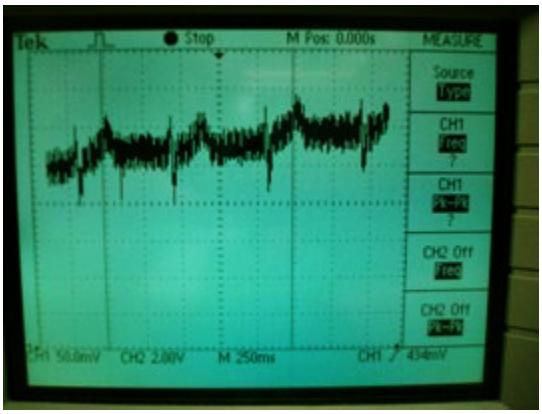


(c)

**Figure 25.** (a) Directly measure from the skin. (b) Measure from one layer of cloth. (c) Measure from two layers of cloths.

# 5.0 SUMMARY OF RESEARCH CONTRIBUTION AND FUTURE WORK

Our experiments and analysis have shown that the proposed approach and system enable direct and non-contact measurement of electric potentials based on spherical volume conductor model. The measurement was realized by capacitor coupling between the electrodes and the inner conducting sphere. Experiments were performed to find the best location and orientation for the electrodes capturing most significant signals. The results match theoretical analysis, which can guide us in future measurement using our capacitive electrodes. The electrodes also showed promising results in measuring real ECG output from the chest.

Although our capacitive electrodes exhibited positive performs in measuring electric potential yielded from both spherical volume conductor model and real ECG output, further research should conducted. Specifically, it is expected to:

1) quantitatively interpret the capacitive coupling effect and its influence on the accuracy of the measurement;
2) conduct signal filtering in either hardware or software to suppress noise and stabilize measurement;
3) design a wearable device to work with electrodes and develop a wireless communication system for signal transmission.

# 6.0 CONCLUSION

In this thesis, the spherical volume conductor model and capacitive electrodes are investigated for the monitoring of ECG signals. The closed-form solution of the spherical volume conductor is utilized in our system design. Although the current dipole is an ideal concept, we demonstrated in Ansoft Maxwell that a dipole can be simulated by metal source and sink separated by an insulator. A dipole antenna and a latex ball containing salted water were constructed to simulate the spherical volume conductor model. The designed capacitive electrodes contain two sensing electrodes and a large reference electrode. As the sensing electrodes measure the local electric potentials, the large reference electrode is used to remove the common noise. Because of the introduction of a differential amplifier, the output of the system provides the potential difference between the two sensing electrodes which can directly measure signals from essentially any locations on the surface of the sphere. Moreover, due to effect of capacitors, the capacitive electrodes are able to capture signals from several layers of cloths. Several experiments were implemented to find best locations to place the electrodes that can detect the most significant signals. The electrodes were also shown to be able to realize both direct and non-contact measurement of the real ECG signals. In addition, the capacitive electrodes were shown that it can obtain most ECG outputs when they were diagonally across the heart.

Although the capacitive electrodes have produced satisfactory results when applying to both spherical volume conductor model and real ECG monitoring, further study is necessary to

improve the measurement stability and accuracy, and to construct a handheld device enclosing the capacitive electrodes.

## BIBLIOGRAPHY


[1] "National Vital Statistics Reports," National Center for Health Statistics2010.

[2] Available: http://en.wikipedia.org/wiki/Ecg

[3] M. Oehler, *et al.*, "Novel multichannel capacitive ECG-System for cardiac diagnostics beyond the standard-lead system," in *4th European Conference of the International Federation for Medical and Biological Engineering*, 2008, p. 4.

[4] M. Oehler, *et al.*, "A multichannel portable ECG system with capacitive sensors," *Physiological Measurement*, vol. 29, pp. 783-793, Jul 2008.

[5] Y. M. Chi and G. Cauwenberghs, "Wireless Non-contact EEG/ECG Electrodes for Body Sensor Networks," presented at the 2010 International Conference on Body Sensor Networks, 2010.

[6] F. N. Wilson and R. H. Bayley, "The Electric Field of an Eccentric Dipole in a Homogeneous Spherical Conducting Medium," *Circulation*, vol. 1, pp. 84-92, 1950.

[7] S. Rush and D. A. Driscoll, "Current Distribution in Brain from Surface Electrodes," *Anesthesia and Analgesia Current Researches*, vol. 47, pp. 717-&, 1968.

[8] B. N. Cuffin and D. Cohen, "Comparison of the Magnetoencephalogram and Electroencephalogram," *Electroencephalography and Clinical Neurophysiology*, vol. 47, pp. 132-146, 1979.

[9] M. G. Sun, "An efficient algorithm for computing multishell spherical volume conductor models in EEG dipole source localization," *Ieee Transactions on Biomedical Engineering*, vol. 44, pp. 1243-1252, Dec 1997.

[10] D. Z. Yao, "Electric potential produced by a dipole in a homogeneous conducting sphere," *Ieee Transactions on Biomedical Engineering*, vol. 47, pp. 964-966, Jul 2000.

[11] G. Dassios, "Electric and Magnetic Activity of the Brain in Spherical and Ellipsoidal Geometry," *Mathematical Modeling in Biomedical Imaging I*, vol. 1983, pp. 133-202, 2009.

[12] G. Dassios and D. Hadjiloizi, "On the non-uniqueness of the inverse problem associated with electroencephalography," *Inverse Problems,* vol. 25, Nov 2009.

[13] J. D. Jackson, *Classical electrodynamics*, 3rd ed. New York: Wiley, 1999.

[14] S. Rush and D. A. Driscoll, "Eeg Electrode Sensitivity - an Application of Reciprocity," *Ieee Transactions on Biomedical Engineering,* vol. Bm16, pp. 15-&, 1969.

[15] M. G. Sun, *et al.*, "Data communication between brain implants and computer," *Ieee Transactions on Neural Systems and Rehabilitation Engineering,* vol. 11, pp. 189-192, Jun 2003.

[16] Available: http://www.vetgo.com/cardio/concepts/concsect.php?sectionkey=5